The Journal of Chemical Physics ARTICLE pubs.aip.org/aip/jcp

Coalescence of liquid or gel-like DNA-encapsulating microdroplets

Cite as: J. Chem. Phys. 161, 134904 (2024); doi: 10.1063/5.0223951
Submitted: 18 June 2024 • Accepted: 19 September 2024 •
Published Online: 2 October 2024

Takashi Nishio[1,a] and Helmut Schiessel[1,2]

AFFILIATIONS

[1] Cluster of Excellence Physics of Life, TUD Dresden University of Technology, 01307 Dresden, Germany
[2] Institut für Theoretische Physik, TUD Dresden University of Technology, 01062 Dresden, Germany

[a] Author to whom correspondence should be addressed: takashinishio7329@gmail.com

ABSTRACT

Liquid–liquid phase separation plays a prominent role in the physics of life, providing the cells with various membrane-less compartments. These structures exhibit a range of material properties that, in many cases, change over time. Inspired by this, we investigate here an aqueous two-phase system formed by mixing polyethylene glycol with dextran. We modulate the material properties of the resulting dextran droplets by adding DNA that readily enters the droplets. We find a non-monotonic dependence of the physical properties of the droplets under the imposed ionic conditions.

I. INTRODUCTION

Liquid–liquid phase separation (LLPS) has recently received much attention as a physical mechanism to regulate the spatial organization in living cells. Cells segregate cellular components such as proteins and nucleic acids via LLPS into micrometer-scale compartments, so-called biomolecular condensates.[1–3] These condensates have membraneless bodies with specific functions and are, therefore, also known as membraneless organelles. Their *in vivo* and *in vitro* material properties, such as their sizes, shapes, and viscosities, vary over a wide range.[4–11] The driving force inducing biomolecular condensates are typically multivalent interactions of the involved biomolecules.[3,12,13] In addition, for some *in vitro* studies,[2] a crowded environment was essential for LLPS to occur as a result of the depletion effect.[2,14–16] This might also play a role in the crowded cellular environment.

As the role of condensates in cells became evident, aqueous two-phase systems (ATPSs), which have been studied for over a century, attracted renewed attention as model systems for macromolecular crowding inside cells.[17–21] ATPSs are systems in which immiscible aqueous solutions are spontaneously separated into two phases above critical concentrations. ATPS has been used to separate various biological materials due to its unique partition ability and, conventionally, ATPS is prepared in a medium-sized vessel. However, recently, ATPS in micrometer-sized spaces has attracted attention, and microdroplets generated near the critical concentration of ATPS are now widely utilized to mimic macromolecular crowding.[17–23] The combination of polyethylene glycol (PEG) and dextran (DEX) leads to one of the most commonly studied ATPSs, and phase diagrams of various combinations of PEG and DEX have been reported.[24] Recently, it has been demonstrated that large-size molecules, such as long double-strand DNA or proteins in an ATPS of PEG and DEX, spontaneously accumulate in DEX-rich microdroplets by mixing.[19–21] This higher selectivity is convenient for creating artificial models of biomolecular condensates and tuning solution conditions. Inspired by these studies, we establish here a simple and cheap model system for biomolecular condensates based on ATPS of PEG and DEX. This system allows to obtain DEX microdroplets that have a DEX-rich solution inside and are surrounded by a PEG-rich solution. We investigate the relationship between the material property of DEX microdroplets, encapsulating λ DNA (48.5 kbp, contour length 16.5 μm), and the spatial organization of DNA as a function of the ionic conditions.

We vary ionic conditions in two ways, by either changing the concentration of monovalent salt or by changing the concentration of spermidine (SPD), a trivalent cation. Spermidine belongs to the polyamines, small polycationic organic molecules that are found in all living organisms. They are involved in many biological functions, such as cell proliferation and differentiation, apoptosis, protection from oxidative damage, and gene regulation.[25] It is well known

that polyamines cause the compaction and condensation of DNA molecules. This, in turn, can affect cell-free gene expression.[26,27] Interestingly, the compaction of DNA accompanied by a change in its volume density on the order of 10^4–10^5 occurs only for giant single DNA molecules, over several tens of kilo base-pairs (kbp);[28] this motivates our choice of the large DNA molecule λ DNA.

II. RESULTS AND DISCUSSION

Figure 1 shows, in the top row, fluorescence microscopy images of DEX microdroplets in the presence of DNA for various concentrations of spermidine (SPD), ranging from 0 to 1.0 mM. Note that we observe DEX microdroplets that are floating in solution far away from the glass surface. To obtain microdroplets, we used 7 wt. % PEG and 1.5 wt. % DEX. The concentration of λ DNA is fixed at 90 μM in nucleotide units, see Sec. IV for details. Based on the fluorescence, it is clear that the DNA is mostly inside the droplets, as has been observed earlier.[19–21] Moreover, the DNA is approximately homogeneously distributed for small SPD concentrations (0, 0.01, and 0.05 mM in Fig. 1) but starts to show regions of increased density for 0.1 mM. For higher concentrations, especially for 1.0 mM, the DNA has collapsed and coalesced into several small aggregates inside the droplets.

We next inspect the droplet shapes in the micrographs of Fig. 1. For small (0 and 0.01 mM) and large (0.5 and 1.0 mM) SPD concentrations, we find spherical droplets. This is expected as the spherical shape maximizes the available free volume for the PEG molecules which drive the droplet formation through depletion. However, for intermediate concentrations of SPD, 0.05 and 0.1 mM, we find many non-spherical-shaped droplets, often being egg-shaped or ellipsoidal. To quantify this, we depict at the bottom of Fig. 1 histograms of the aspect ratios of the droplets, which clearly support this finding. For 0 and 0.01 mM and for 0.5 and 1.0 mM SPD, all the droplets fall in the first bin of the diagram, i.e., feature aspect ratios not larger than 1.05. However, for 0.05 and 0.1 mM, there are many droplets that have larger aspect ratios. This is especially striking for 0.1 mM SPD featuring a local peak at bin 1.15–1.2.

Note that SPD is a trivalent counterion whose binding is caused by the release of monovalent counterions that are condensed on the DNA double helix.[28–31] The bound SPD ions cause a self-attraction of the DNA molecule via correlation-induced attraction,[28,29,32–34] which are known to lead to various condensed structures of DNA, such as toroids, flower-like structures, multi-chain aggregates, and liquid crystalline phases.[26,28,35–37] We next reduce the entropy gain by counterion release by adding NaCl[27] and then study the effect on the droplet shape. In Fig. 2(a), we depict an array of micrographs of DEX droplets with DNA. The left column shows micrographs in the absence of SPD, the middle column for 0.1 mM, and the right column for 1.0 mM SPD. In the vertical direction, we increase the amount of added NaCl. Specifically, the first row shows micrographs in the absence of added NaCl, the second row for 0.1 mM NaCl, and, further for each row, the NaCl concentration is ten-fold increased up to 100 mM in the fifth row. Without SPD (left column), we observe spherical droplets containing homogeneously distributed DNA for all NaCl concentrations. The top of the middle column (0.1 mM, no salt) corresponds to non-spherical droplets and non-homogeneously distributed DNA. With increasing NaCl concentration, the DNA density within the droplets becomes homogeneous at about 1 mM NaCl. Moreover, we find non-spherical droplets for the four smaller salt concentrations and spherical shapes for 100 mM. Finally, in the right column, 1.0 mM SPD, we observe strongly compacted DNA aggregates inside spherical droplets for the smaller four NaCl concentrations, whereas at

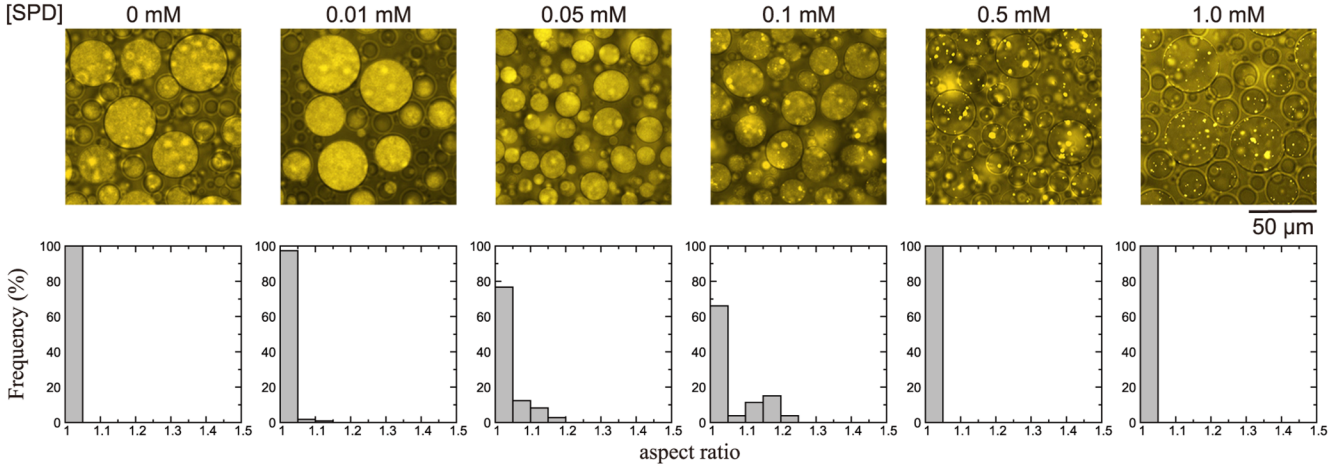

FIG. 1. Typical fluorescence microscopy images and aspect ratio distributions of DEX microdroplets (7 wt. % PEG and 1.5 wt. % DEX) entrapping λ DNA molecules at different SPD concentrations. The DNA concentration was fixed at 90 μM in nucleotide units. We measured the aspect ratios of more than 50 individual droplets under each experimental condition from the ellipse approximation by using the particle analysis function of ImageJ. We binned all shapes with aspect ratio of 1–1.05 in the first bar and so on. The heights of the bars give the percentages that the corresponding shapes were observed.

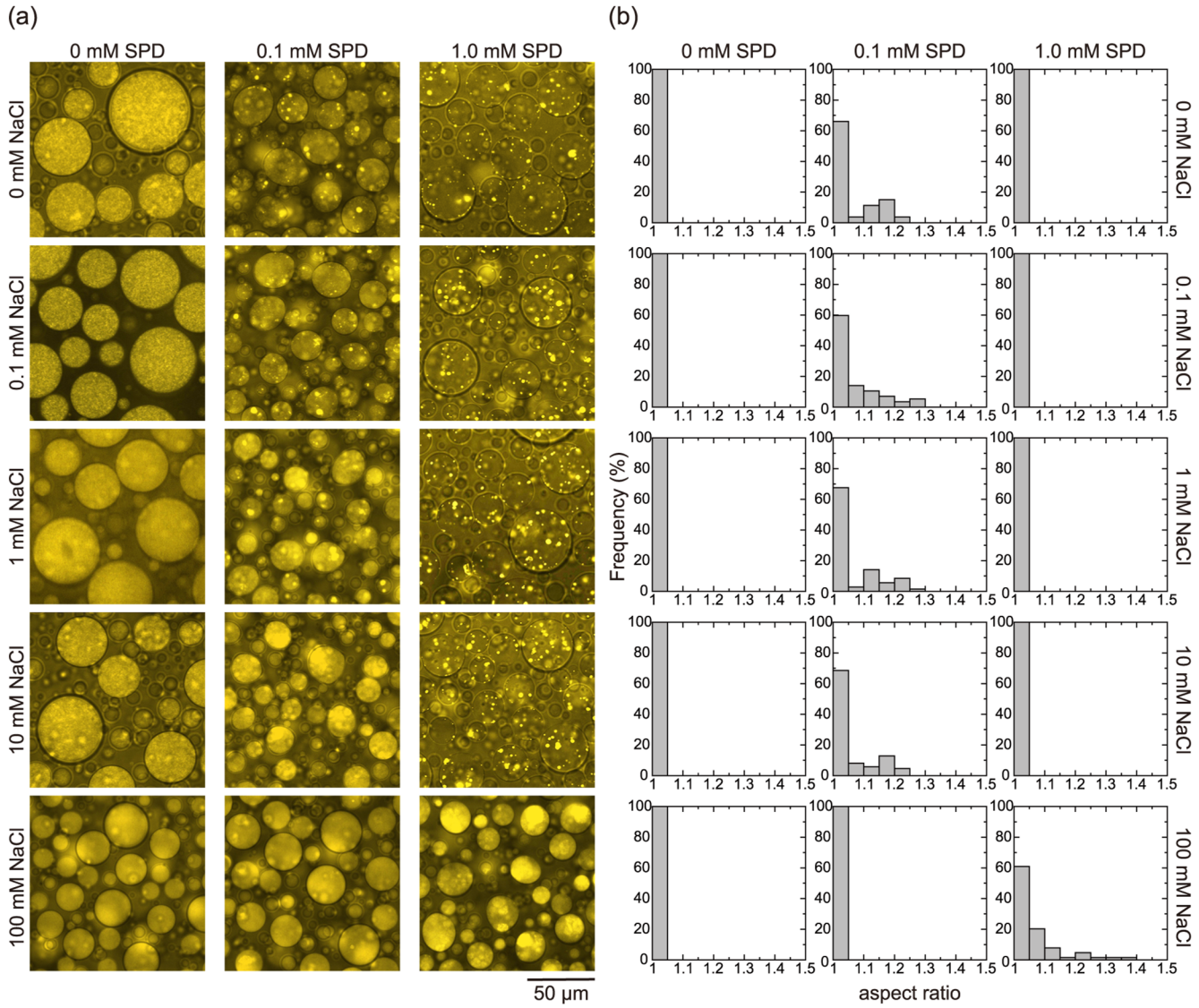

FIG. 2. Typical fluorescence microscopy images (a) and aspect ratio distributions (b) of DEX microdroplets entrapping λ DNA molecules at different SPD and NaCl concentrations. The DNA concentration was fixed at 90 μM in nucleotide units. Aspect ratios were determined as shown in Fig. 1.

the highest salt concentration, DNA is homogeneously distributed and droplets are non-spherical. These conclusions are confirmed quantitatively in Fig. 2(b) that displays the distributions of aspect ratios for all 15 ionic conditions. Overall, the observed changes in the DNA distributions inside the droplets shown in Fig. 2(a) are consistent with the electrostatic mechanisms of counterion release and correlation-induced attraction.

To understand better the overall conformations of the DNA molecules inside the droplets and how they affect the droplet shape, we characterize, in the following, the material properties of the droplets as a function of the concentration of SPD and NaCl. These can be extracted from droplet fusion events like the one shown in Fig. 3. From the speed of droplet coalescence, one can extract a combination of physical parameters of the condensates, namely the ratio η/γ with η being the drop viscosity (which needs to be larger than the viscosity of the surrounding medium) and γ being the surface tension. Conventionally, this quantity is extracted for biomolecular condensates by fitting an exponential function to the temporal development of the aspect ratio.[4–10] However, given the complex geometry of two fusing droplets, it is unlikely that such a simple relation fits the data well. For instance, the fusion curve of two droplets from the *C. elegans* protein PGL-3[11] suggests that the aspect ratio does not follow a simple exponential decay, see blue curve in their Fig. 1(d).

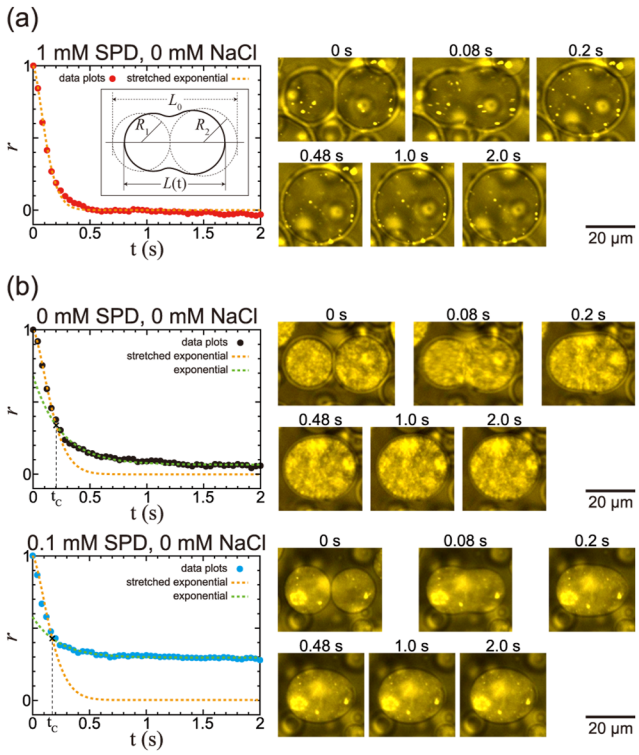

FIG. 3. Analysis of shape change dynamics of DEX droplets. (a) and (b) The fitting by using both stretched exponential ($r = e^{-(t/\tau_f)^\beta}$) and exponential ($r = ae^{-t/\tau_r} + b$) or only stretched exponential for the time course of the edge-to-edge distance $r = (L(t) - L_\infty)/(L_0 - L_\infty)$. τ_f, τ_r, a, and b are fitting parameters, and $\beta = 1.5$.

In fact, Ghosh and Zhou[38] found recently that the decay of the edge-to-edge distance $L(t)$ of two fusing droplets [see inset of Fig. 3(a)] can be well approximated by a stretched exponential,

$$\frac{L(t) - L_\infty}{L_0 - L_\infty} = e^{-(t/\tau_f)^\beta}, \tag{1}$$

where L_0 is the edge-to-edge distance of the two spherical droplets in contact before the onset of fusion and L_∞ is the diameter of the fused droplet, assuming it relaxes into a spherical shape. The exponent β is not universal but depends on the fusion time τ_f; the authors of Ref. 38 propose $\beta = 1.5$ as a good compromise for which $\tau_f = 1.97(\eta/\gamma)\left(L_\infty/2^{4/3}\right)$.

The fusion dynamics for the ionic conditions shown in the top row of Fig. 2 are exemplified in Fig. 3. For 1.0 mM SPD and 0 mM NaCl, Fig. 3(a), the edge-to-edge distance follows strikingly well a stretched exponential, Eq. (1). This is also the case for DEX droplet fusion without DNA, see Fig. S1(b). These curves are not simple exponentials, as can be best seen when inspecting semi-log plots. For example, the red data points shown in Fig. 4(a) for 0 mM NaCl, which lie along a curved line. On the other hand, rewriting Eq. (1) in terms of the aspect ratio A.R. suggests a rather complicated functional dependence,

$$\text{A.R.} = \left(\left(\frac{L_0}{L_\infty} - 1\right)e^{-(t/\tau_f)^\beta} + 1\right)^{3/2}, \tag{2}$$

which, together with the complications of fitting an ellipsoid to two fusing droplets, suggests that the edge-to-edge distance is a more natural quantity for describing droplet fusion than the aspect ratio.

The situation is more complex for most conditions considered in this study. An example is the coalescence curve in the absence of SPD and without added salt, Fig. 3(b)—top row. The initial part of the curve up to a crossover time t_c, here about 0.2 s, follows a stretched exponential. For times larger than t_c, however, the fusion dynamics is slowed down substantially. In fact, it can be well described by an ordinary exponential. Moreover, the crossover is rather sharp and is well-defined by the intersection of the stretched and ordinary exponential curves.

We hypothesize that the first part of the fusion is not much hindered by the presence of the DNA inside the droplets and can, thus, be well described by a stretched exponential. When DNA is compacted into tight aggregates, as is the case in Fig. 3(a), this behavior continues indefinitely, as if DNA were not present. However, under most ionic conditions considered here, DNA slows down the further recovery to a final spherical droplet or even stops the process before the spherical shape is reached. The independence of the initial part of the fusion dynamics from the DNA state could also be a result of shear thinning. As the initial internal flow in the droplet shows large shear rates, DNA molecules might be stretched which disentangles the molecules. In fact, it has been shown by bulk rheological measurements of a DEX-rich phase containing coiled DNA that the dynamic viscosity is reduced to values close to that of DEX with globular DNA or in the absence of DNA [see Fig. 6(d) in Ref. 39]. Whether shear thinning applies for such a small-scale motion as in our droplets, remains, however, an open question. In any case, given the sharp transition, we assume the first section of the curve to reflect the viscosity of the DEX droplet (independent of the DNA) and the second for the higher viscosity of the DEX/DNA droplet.

We discuss now the slow section of the coalescence curve. In Ref. 40, Zhou gave exact analytical solutions for the shape recovery of deformed droplets and found that for cases where the friction of the outer fluid can be neglected,

$$\frac{L(t) - L_\infty}{L(t_c) - L_\infty} = e^{-t/\tau_r}, \tag{3}$$

with a recovery time $\tau_r = (19/40)(\tilde{\eta}/\gamma)L_\infty$. Here, $\tilde{\eta}$ is the viscosity of the DEX/DNA droplet. Assuming the surface tension γ to be unaltered by the presence of the DNA [see Fig. 6(c) in Ref. 39], we can detect directly how the effective viscosity of the droplet changes. In principle, the formalism of Ref. 40 allows also to account for viscoelastic effects. Describing, e.g., the droplet as viscoelastic via the Jeffrey model modifies Eq. (3) to a sum of two exponentials.[40] Although some of our data show hints of a slower decay at long times [see Fig. 4(a)], they only allow to fit the fast decaying component. To a good approximation, this component has the time constant τ_r from above.[40]

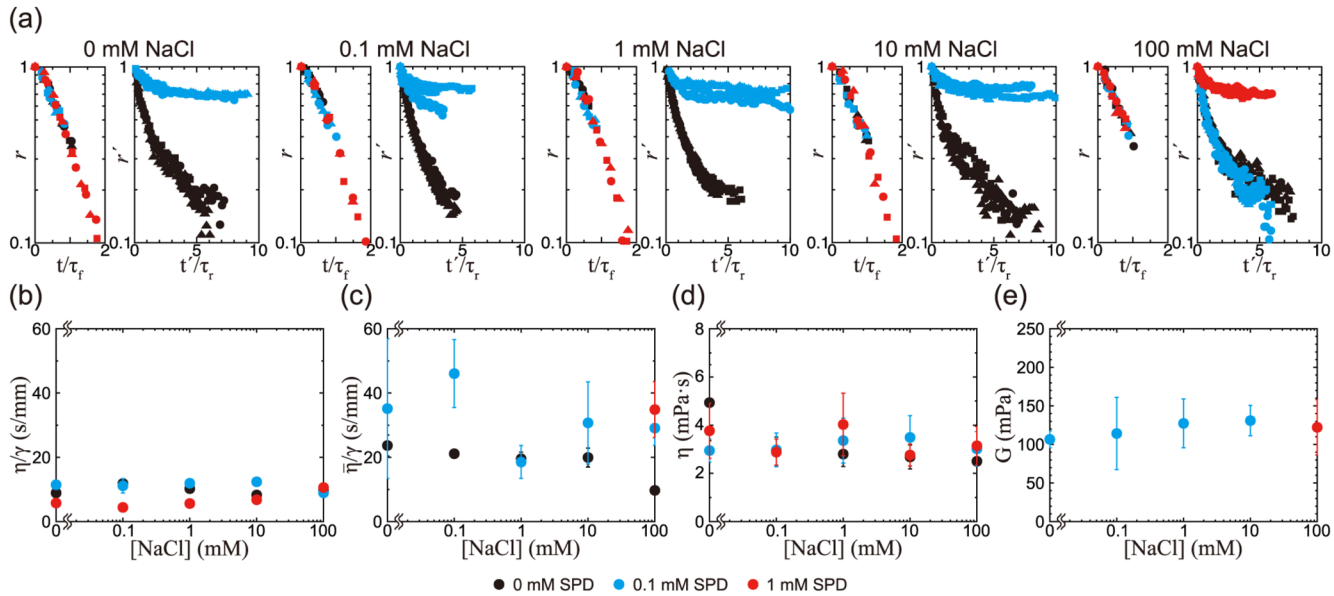

FIG. 4. Viscoelastic analysis of microdroplets. (a) Universal plots of the edge-to-edge distance vs time rescaled by τ_f or τ_r at various concentrations of SPD and NaCl. r' and t' are normalized to be (1, 0) at $t = t_c$. Three individual droplets were analyzed for each condition. (b) and (c) Ratios η/γ and $\bar{\eta}/\gamma$ determined from the fit parameters τ_f and τ_r. (d) Viscosity η measured by single particle tracking technique under the various ionic conditions. (e) Elastic module G for the cases of arrested coalescence.

Using Eqs. (1) and (3), we produce dimensionless plots in Fig. 4(a). Specifically, we plot for each concentration of NaCl the dimensionless edge-to-edge distance $r = (L(t) - L_\infty)/(L_0 - L_\infty)$ as a function of t/τ. In these plots, we present the stretched exponential and the simple exponential sections separately with the time rescaled by the corresponding τ, τ_f, and τ_r, respectively. The reason not to combine them into one master plot is that the ratio η/γ changes when one crosses from the DEX-dominated stretched exponential regime to the DNA-dominated exponential regime. Moreover, for the right panels, we shift the time by the crossover time t_c and rescale r such that it has the value 1 at $t = t_c$. For each of the different ionic conditions, we show relaxation curves from three different fusion events. Overall, the data points from these three events collapse on corresponding master curves.

Moreover, under conditions in which we observe non-spherical droplets, we find that r does not relax to zero, but rather that $L(t) - L_\infty$ approaches a finite plateau, see Fig. 3(b)—bottom row. This suggests that the droplet has a finite elasticity because the DNA molecules are crosslinked by SPD into a DNA gel which, at least on the time scale of the experiment, does not rearrange its connectivity. We speculate that this situation arises at intermediate SPD concentrations. For higher concentrations, there is enough SPD to collapse the DNA molecules into tight aggregates, and for low concentrations, there is not enough SPD to crosslink the DNA molecules into a network that spans the whole droplet.

To determine the shear modulus from this arrested coalescence, we find the edge-to-edge distance $L = L_{\min}$ that minimizes the total energy.[41] There are two relevant contributions. The first contribution is the surface energy E_S of the droplet, which we assume to be a prolate ellipsoid with constant volume. An expansion in the lowest order in $D = (L - L_\infty)/L_\infty$ yields $E_S = \pi\gamma L_\infty^2\left(1 + 2D^2/5\right)$. The second contribution is the elastic energy E_{elas}. Based on the observation discussed above that the DNA slows down the fusion dynamics for times larger than the crossover time t_c, we assume that the DNA network is still in its undeformed state at $t = t_c$. The elastic energy is then $E_{elas} = 2\pi G\epsilon^2 L_\infty^3$ with G denoting the shear modulus and $\epsilon = (L - L(t_c))/L(t_c)$.[41] The droplet energy is minimized for

$$L_{\min} = \frac{1}{1+A}\left(L_\infty + AL(t_c)\right), \tag{4}$$

with $A = (5/8)(G/\gamma)L_\infty^3/L(t_c)^2$.

To determine G from A, we need to know the surface tension γ. However, the fusion experiments provide only the ratios η/γ and $\bar{\eta}/\gamma$ for various conditions, see Figs. 4(b) and 4(c). To estimate γ from these data, we measure η directly using single particle tracking[6,8,9,11,21] (see Sec. IV), leading to η-values between 2 and 6 mPa s, as shown in Fig. 4(d). Therefore, our DEX droplets have viscosities higher than water (0.89 mPa s) at room temperature (25 °C).[42] Our analysis suggests that γ is not sensitive to ionic conditions, see Fig. S2. Therefore, we determine its value from the average over all conditions, leading to a γ-value of 0.396 ± 0.126 μN/m. With this, we estimate the elastic modulus G for various conditions from Eq. (4), see Sec. IV for details. As shown in Fig. 4(e), G has values between 100 and 150 mPa. This is much smaller than the G-values in the range of 10–50 Pa of aged biomolecular condensates (PGL-3) reported by Jawerth *et al.*[11] On the other hand, the values of G in droplets with arrested coalescence are comparable to values of the plateau modulus measured for entangled DNA solutions.[43] In addition, Fig. 4(e) suggests that for all ionic conditions where

we observe non-spherical droplets, the elastic modulus has a similar value. Taken together, this indicates a switch-like behavior of DEX droplets containing DNA. Depending on the ionic conditions, one has either a DNA gel with constant crosslink density or rather liquid-like behavior when the DNA molecules either form collapsed globules or are dissolved inside the droplets.

III. CONCLUSIONS

In summary, our measurements demonstrate that DNA and multivalent ions, such as SPD, can be used to control the viscoelastic properties of droplets formed in an aqueous two-phase system. We found a non-monotonic behavior of the droplet properties with the concentration of SPD. We speculate that this reflects the formation of a DNA network at intermediate SPD concentrations. On the time scale of our experiment, the fusion of these droplets is arrested, whereas for other conditions, i.e., for low and high concentrations of SPD, the fused droplet relaxes quickly into a spherical shape. The addition of monovalent ions shifts the onset of the regime with finite elasticity to larger SPD concentrations. Overall, these findings were obtained from droplet fusion measurements and from single particle tracking, which allowed us to extract all relevant material properties of the droplets. We expect that this simple model system will serve as a platform to test ideas on biomolecular condensates that play a crucial role in the phase behavior in biological cells.

IV. MATERIALS AND METHODS

A. Materials

Polyethylene glycol (PEG) of 6 kDa, dextran (DEX) of 200 kDa, tris-hydrochloride acid buffer (pH 7.5), spermidine trihydrochloride (SPD), and sodium chloride (NaCl) were purchased from Sigma-Aldrich (MO, USA). λ DNA (48.5 kbp with a contour length of ~16.5 μm in aqueous solution) and dithiothreitol (DTT) were purchased from Thermo Fisher Scientific (MA, USA). The dimeric cyanine fluorescent dye YOYO-1 (1,10-(4,4,7,7-tetramethyl-4,7-diazaundecamethylene)bis[4-[(3-methylbenzo-1,3-oxazol-2-yl)methylidene]-l,4 dihydroquinolinium] tetraiodide) was obtained from Invitrogen (MA, USA).

B. Preparation of microdroplets

To prepare DEX microdroplets, we adopted an aqueous two-phase system by using 7 wt. % PEG and 1.5 wt. % DEX, which is close to the bimodal line in the phase diagram.[19] DEX microdroplets, which have a DEX-rich solution inside the droplet and are surrounded by a PEG-rich solution, are generated spontaneously with the solution becoming cloudy after mixing it with a vortex mixer. λ DNA molecules are spontaneously entrapped into DEX-rich droplets by simply mixing with a vortex mixer. Fluorescence microscopy (FM) observations were conducted at DNA concentrations of 90 μM (in nucleotide units) with the addition of 0.5 μM YOYO-1. The final concentrations of other compounds were 10 mM Tris-HCl buffer solution at pH 7.5, 10 mM DTT, and the desired concentrations of SPD and NaCl.

C. Fluorescence microscopy observation

We performed FM observations by using an inverted fluorescence microscope (ECLIPSE Ti2, Nikon, Tokyo, Japan) with a 60× water-immersion objective lens (SR Plan Apo IR, NA 1.27, Nikon, Tokyo, Japan). Fluorescent illumination was performed using a laser light source with a confocal scanner unit (CSU-W1, YOKOGAWA, Tokyo, Japan). To visualize both DNA molecules and contours of microdroplets simultaneously, we performed the observation under constant transmitted light. We recorded the images at 25 or 100 f/s through a CMOS camera (ORCA-Fusion BT, Hamamatsu Photonics, Shizuoka, Japan). We analyzed images with the image-processing software ImageJ (National Institute of Mental Health, MD, USA).

D. Fusion analysis

As explained in Fig. 3, we carried out the fitting of the time course of the dimensionless edge-to-edge distance $r = (L(t) - L_\infty)/(L_0 - L_\infty)$ of fusing droplets by using a stretched exponential curve [Eq. (1)] and an exponential curve [Eq. (3)] based on the least squares method. The equations that we used for fitting are the following:

$$r = e^{-(t/\tau_f)^\beta} \tag{5}$$

and

$$r = ae^{-t/\tau_r} + b. \tag{6}$$

Following Ref. 38, we set $\beta = 1.5$. The other parameters, τ_f, τ_r, a, and b, are fitting parameters. We note that the fitting parameter a in Eq. (6) contains a prefactor that was generated when Eq. (3) was converted into the form of Eq. (6). We introduced the fitting parameter b to fit data where r did not reach 0, i.e., where the final shape was not spherical. b is given by the edge-to-edge distance that minimizes the total energy, $L_{\min}$, $b = (L_{\min} - L_\infty)/(L_0 - L_\infty)$. For the data with 1 mM SPD (except in the case of 100 mM NaCl) and the data without DNA (Fig. S1), all the data points were fitted by the stretched exponential curve alone. All other data were fitted by both the stretched exponential curve and the exponential curve. The stretched exponential curve was used for fitting the beginning part of the fusion curve, using at least five data points, whereas the rest was fitted by the exponential curve. To determine the appropriate crossover point, we increased the data points fitted by the stretched exponential one by one until the residual sum of squares of all data started to grow. From the optimal fit, we calculated the crossover time t_c from the intersection of the two fitting curves.

E. Viscosity analysis: Single particle tracking

The fusion analysis allows only to determine the ratio η/γ. To extract the droplet viscosity, we tracked single microspheres inside the droplets. The dextran molecules have a hydrodynamic radius of about 11.6 nm.[44] The diameter of our bead is 0.5 μm, which is roughly 25 times the size of a dextran molecule. This means that we measure the properties of the dextran solution. The droplets can be considered stationary on the relevant time scales (≤0.5 s, see below): the rotational relaxation time of a droplet of the typical size found

in our experiment (10 μm radius) is about 45 min in water, and it will take three times longer before the mean-squared displacement (MSD) reaches its own diameter. Since we seal the observation chamber, there is also no flow inside the sample.

Figure S3 shows the MSD curves of microbeads inside droplets for all ionic conditions. Each curve is an average of over ten trajectories. In addition, for each time point, we average over all available corresponding time intervals. The first part of each trajectory (its first third or half) suggests a linear dependence, as expected from diffusion. Beyond that, the trajectories seem to deviate in random directions from the linear behavior. We checked with computer simulations of ordinary diffusion using the same number of "measurement" points that comparable MSDs are also observed in this case, suggesting that deviations of the MSD curves from linear behavior simply reflect random fluctuations due to small numbers. If the dextran droplets were viscoelastic, we would expect systematic deviations from the linear behavior of the MSD.[45] Moreover, we note that the microbeads are hardly affected by the presence of DNA, even for the crosslinked gel, indicating that the beads can diffuse freely inside the droplets under all experimental conditions. This behavior is expected for cases where the bead is smaller than the correlation length of the DNA solution or the typical meshwork size of the crosslinked DNA gel.[46,47]

For one experimental condition, we also tracked the motion of the centers of mass of three microdroplets. The resulting MSD curve is shown in red in Fig. S3. Displacements are about two orders of magnitude smaller than the ones of the microbeads. This demonstrates that drift or noise in our experimental setup are at negligible levels, allowing us to reliably track single microbeads.

Even though the trajectories in Fig. S3 are compatible with ordinary diffusion, we noted that the system behaves more complexly. We observed that microspheres got occasionally trapped in the DEX or DNA network presumably because of the high concentrations of these macromolecules. To account for this, we divided each trajectory of the microspheres into shorter segments from which we determined viscosities individually. Specifically, we divided the 10 s trajectories into 20 0.5 s short time intervals as shown in Fig. 5.

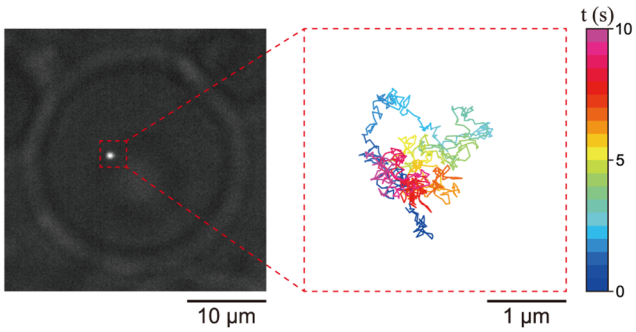

FIG. 5. Estimating the DEX microdroplet viscosity from single particle tracking. Left: Fluorescence microscopy image of microsphere inside DEX microdroplets in the absence of λ DNA, SPD, and NaCl. Right: Trajectory of microsphere shown on the left side for a 10 s time interval. The trajectory was divided into 20 sub-trajectories and the viscosity was calculated individually from the mean square displacement using the Stokes–Einstein relation.[48] The analysis was carried out with ten individual microdroplets for each condition. The frame rate of the movies was 100 frames/s.

We note that the frame rate of our movies was 100 frames/s so that each time interval provided 50 data points. We plotted the mean square displacement (MSD) from individual sub-trajectories and determined the diffusion coefficient D from the relation between the MSD and the lag time Δt for the simple case of Brownian motion in two dimensions,[49]

$$MSD(\Delta t) = 4D\Delta t. \tag{7}$$

To have good statistics, we used only lag times up to 0.05 s for each sub-trajectory. The viscosity η was then determined by using the Stokes–Einstein relation,[48]

$$\eta = \frac{k_B T}{6\pi D R}, \tag{8}$$

where k_B is the Boltzmann constant, T = 298 K, and R is the radius of the microsphere, 0.25 μm. We obtained 20 viscosity values from the trajectory of an identical microsphere in a microdroplet and analyzed ten individual microdroplets for each condition. This means that we obtained a total of 200 viscosity values for each condition. Fig. S4 shows histograms of the measured viscosities for each condition. We fitted the distributions of viscosities for each condition with a Gaussian mixture distribution that is constructed of three Gaussian distributions. The resulting fits for different concentrations of SPD and NaCl are shown in Fig. S4. We observed typically two peaks whose relative height is systematically shifted with the addition of NaCl and SPD, with the lower viscosity component becoming prominent. This might reflect reduced interaction between the bead and the macromolecules due to electrostatic screening. We assume, in the following, that the lower viscosity is relevant for the initial droplet fusion. Obtained mean η-values for each condition were in the range from 2 to 6 mPa s [see Fig. 4(d)]. This value is reasonable in comparison with other studies that have determined the viscosity of DEX droplets.[21,44,47]

F. Calculation of elastic modulus G

To determine G from A defined below Eq. (4), we first estimate $\langle\gamma\rangle$ for each SPD and NaCl concentration. To do this, we divide for each ionic condition the ratio $\langle\eta/\gamma\rangle$, averaged over three fusion events, Fig. 4(b), by $\langle\eta\rangle$ measured from the single particle trajectories, Fig. 4(d). The result of this operation is shown in Fig. S2. This plot suggests that γ is not sensitive to the ionic conditions. We, therefore, determine its value from the average over all conditions, leading to an estimate for γ given by $\langle\langle\gamma\rangle\rangle = 0.399 \pm 0.126$ μN/m. The standard deviation, $\sigma_{\langle\langle\gamma\rangle\rangle}$, is the average over individual standard deviations of $\langle\gamma\rangle$, $\sigma_{\langle\gamma\rangle}$, for each ionic condition. Here, $\sigma_{\langle\gamma\rangle}$, the error propagation was calculated using the variance formula as follows:

$$\sigma_{\langle\gamma\rangle} = \sqrt{\left(\frac{1}{\langle\eta/\gamma\rangle}\right)^2 \sigma^2_{\langle\eta\rangle} + \left(-\frac{\langle\eta\rangle}{\langle\eta/\gamma\rangle^2}\right)^2 \sigma^2_{\langle\eta/\gamma\rangle}}. \tag{9}$$

SUPPLEMENTARY MATERIAL

The supplementary material encompasses: Figure S1. DEX microdroplets without λ DNA molecules, SPD, and NaCl. (a) Typical bright-field microscopy image and aspect ratio distribution. Aspect ratios were determined as in Fig. 1. (b) Example of fitting of the time course of the edge-to-edge distance $r = (L(t) - L_\infty)/(L_0 - L_\infty)$ by a stretched exponential. (c) Series of bright-field microscopy images of two fusing microdroplets. (d) Edge-to-edge distance vs dimensionless time t/τ_f for three individual droplet fusion events. Figure S2. Surface tension γ under various ionic conditions. γ was estimated from η/γ determined by the analysis of droplets fusion and η measured by single particle tracking. Figure S3. Plots of the mean squared displacement (MSD) of microbeads. Individual MSDs were determined from microbead trajectories in ten different microdroplets for each experimental condition. For each microbead, we tracked the 10-s trajectory of one microbead. In addition, the red curve shows the MSD of the microdroplet center of mass. The curve was obtained by averaging over 10 second trajectories of the centers of mass of three microdroplets. The inset shows the same curve displayed with a smaller vertical axis range. Figure S4. Histograms of the viscosity of DEX microdroplets obtained by a single particle tracking technique in the presence of various SPD and NaCl conditions. Histograms were fitted by a Gaussian mixture distribution that is constructed of three Gaussian distributions. Movie S1. Coalescence of two DEX microdroplets without λ DNA in the absence of neither SPD nor NaCl. Movie recorded at 25 f/s. Movie S2. Coalescence of two DEX microdroplets encapsulating λ DNA in the absence of neither SPD nor NaCl. DNA concentration was fixed at 90 μM in nucleotide unit. Movie recorded at 25 f/s. Movie S3. Coalescence of two DEX microdroplets encapsulating λ DNA in the presence of 0.1 mM SPD. DNA concentration was fixed at 90 μM in nucleotide unit. Movie recorded at 25 f/s. Movie S4. Coalescence of two DEX microdroplets encapsulating λ DNA in the presence of 1 mM SPD. DNA concentration was fixed at 90 μM in nucleotide unit. Movie recorded at 25 f/s

ACKNOWLEDGMENTS

The authors thanked Arash Nikoubashman for insightful discussions. T.N. and H.S. were supported by the Deutsche Forschungsgemeinschaft (DFG, German Research Foundation) under Germany's Excellence Strategy—No. EXC-2068—390729961. This work was partially supported by JSPS KAKENHI Grants (Nos. JP22K20640 and JP23K14159 to T.N.) and by grants from the Uehara Memorial Foundation (to T.N.).

AUTHOR DECLARATIONS

Conflict of Interest

The authors have no conflicts to disclose.

Author Contributions

Takashi Nishio: Conceptualization (equal); Data curation (equal); Formal analysis (equal); Funding acquisition (equal); Investigation (equal); Methodology (equal); Writing – original draft (equal); Writing – review & editing (equal). **Helmut Schiessel**: Conceptualization (equal); Funding acquisition (equal); Methodology (equal); Supervision (equal); Writing – original draft (equal); Writing – review & editing (equal).

DATA AVAILABILITY

The data that support the findings of this study are available within the article and its supplementary material.

REFERENCES

[1] A. A. Hyman, C. A. Weber, and F. Jülicher, Annu. Rev. Cell Dev. Biol. **30**, 39 (2014).
[2] A. A. M. André and E. Spruijt, Int. J. Mol. Sci. **21**, 5908 (2020).
[3] B. Wang, L. Zhang, T. D. Z. Qin, H. Lu, L. Zhang, and F. Zhou, Signal Transduction Targeted Ther. **6**, 290 (2021).
[4] C. P. Brangwynne, T. J. Mitchison, and A. A. Hyman, Proc. Natl. Acad. Sci. U. S. A. **108**, 4334 (2011).
[5] A. Hubstenberger, S. L. Noble, C. Cameron, and T. C. Evans, Dev. Cell **27**, 161 (2013).
[6] S. Elbaum-Garfinkle, Y. Kim, K. Szczepaniak, C. C. Chen, C. R. Eckmann, S. Myong, and C. P. Brangwynne, Proc. Natl. Acad. Sci. U. S. A. **112**, 7189 (2015).
[7] A. Patel, H. O. L. L. Jawerth, S. Maharana, M. Jahnel, M. Y. Hein, S. Stoynov, J. Mahamid, S. Saha, T. M. Franzmann, A. Pozniakovski, I. Poser, N. Maghelli, L. A. Royer, M. Weigert, E. W. Myers, S. Grill, D. Drechsel, A. A. Hyman, and S. Alberti, Cell **162**, 1066 (2015).
[8] H. Zhang, S. Elbaum-Garfinkle, E. M. Langdon, N. Taylor, P. Occhipinti, A. A. Bridges, C. P. Brangwynne, and A. S. Gladfelter, Mol. Cell **60**, 220 (2015).
[9] M. Feric, N. Vaidya, T. S. Harmon, D. M. Mitrea, L. Zhu, T. M. Richardson, R. W. Kriwacki, R. V. Pappu, and C. P. Brangwynne, Cell **165**, 1686 (2016).
[10] S. Boeynaems, A. S. Holehouse, V. Weinhardt, D. Kovacs, J. Van Lindt, C. Larabell, L. Van Den Bosch, R. Das, P. S. Tompa, R. V. Pappu, and A. D. Gitler, Proc. Natl. Acad. Sci. U. S. A. **116**, 7889 (2019).
[11] L. Jawerth, E. Fischer-Friedrich, S. Saha, J. Wang, T. Franzmann, X. Zhang, J. Sachweh, M. Ruer, M. Ijavi, S. Saha, J. Mahamid, A. A. Hyman, and F. Jülicher, Science **370**, 1317 (2020).
[12] S. F. Banani, H. O. Lee, A. A. Hyman, and M. K. Rosen, Nat. Rev. Mol. Cell Biol. **18**, 285 (2017).
[13] S. Alberti, A. Gladfelter, and T. Mittag, Cell **176**, 419 (2019).
[14] S. Asakura and F. Oosawa, J. Polym. Sci. **33**, 183 (1958).
[15] M. Surve, V. Pryamitsyn, and V. Ganesan, J. Chem. Phys. **122**, 154901 (2005).
[16] J. Groen, D. Foschepoth, E. T. Brinke, A. J. Boersma, H. Imamura, G. Rivas, H. A. Heus, and W. T. S. Huck, J. Am. Chem. Soc. **137**, 13041 (2015).
[17] Y. Li, R. Lipowsky, and R. Dimova, Proc. Natl. Acad. Sci. U. S. A. **108**, 4731 (2011).
[18] C. D. Keating, Acc. Chem. Res. **45**, 2114 (2012).
[19] K. Tsumoto, M. Arai, N. Nakatani, S. N. Watanabe, and K. Yoshikawa, Life **5**, 459 (2015).
[20] N. Nakatani, H. Sakuta, M. Hayashi, S. Tanaka, K. Takiguchi, K. Tsumoto, and K. Yoshikawa, ChemBioChem **19**, 1370 (2018).
[21] T. Nishio, Y. Yoshikawa, and K. Yoshikawa, PLoS One **16**, e0261736 (2021).
[22] W. Guo, A. B. Kinghorn, Y. Zhang, Q. Li, A. D. Poonam, J. A. Tanner, and H. C. Shum, Nat. Commun. **12**, 3194 (2021).
[23] Q. Chen, Y. Zhang, H. Chen, J. Liu, and J. Liu, Anal. Chem. **93**, 8577 (2021).
[24] P. A. Albertson, *Partition of Cell Particles and Macromolecules*, 2nd ed. (John Wiley & Sons, Inc., 1972).
[25] A. K. Handa, T. Fatima, and A. K. Mattoo, Front. Chem. **6**, 10 (2018).
[26] T. Nishio, Y. Yoshikawa, C.-Y. Shew, N. Umezawa, T. Higuchi, and K. Yoshikawa, Sci. Rep. **9**, 14971 (2019).
[27] T. Nishio, K. Sugino, Y. Yoshikawa, M. Matsumoto, Y. Oe, K. Sadakane, and K. Yoshikawa, PLoS One **15**, e0238447 (2020).

[28]K. Yoshikawa and Y. Yoshikawa, *Pharmaceutical Perspectives of Nucleic Acid-Based Therapy*, 1st ed. (CRC Press, London, 2002), Chap. 8.
[29]H. Schiessel, *Biophysics for Beginners: A Journey through the Cell Nucleus*, 2nd ed. (Jenny Stanford Publishing Pte Ltd., 2022).
[30]G. S. Manning, Q. Rev. Biophys. **11**, 179 (1978).
[31]J. Widom and R. L. Baldwin, J. Mol. Biol. **144**, 431 (1980).
[32]I. Rouzina and V. A. Bloomfield, J. Phys. Chem. **100**, 9977 (1996).
[33]A. Naji, S. Jungblut, A. G. Moreira, and R. R. Netz, Physica A **352**, 131 (2005).
[34]M. L. Henle and P. A. Pincus, Phys. Rev. E **71**, 060801 (2005).
[35]V. A. Bloomfield, Biopolymers **44**, 269 (1997).
[36]M. Saminathan, T. Thomas, A. Shirahata, C. K. S. Pillai, and T. J. Thomas, Nucleic Acids Res. **30**, 3722 (2002).
[37]T. Iwataki, S. Kidoaki, T. Sakaue, K. Yoshikawa, and S. S. Abramchuk, J. Chem. Phys. **120**, 4004 (2004).
[38]A. Ghosh and H.-X. Zhou, Angew. Chem., Int. Ed. **59**, 20837 (2020).
[39]T. Furuki, H. Sakuta, N. Yanagisawa, S. Tabuchi, A. Kamo, D. S. Shimamoto, and M. Yanagisawa, ACS Appl. Mater. Interfaces **16**, 43016 (2024).
[40]H.-X. Zhou, J. Chem. Phys. **155**, 145102 (2021).
[41]A. B. Pawar, M. Caggioni, R. W. Hartel, and P. T. Spicer, Faraday Discuss. **158**, 341 (2012).
[42]L. Korson, W. Drost-Hansen, and F. J. Millero, J. Phys. Chem. **73**, 34 (1969).
[43]X. Zhu, B. Kundukad, and J. R. C. van der Maarel, J. Chem. Phys. **129**, 185103 (2008).
[44]K. Harusawa, C. Watanabe, Y. Kobori, K. Tomita, A. Kitamura, M. Kinjo, and M. Yanagisawa, Langmuir **37**, 437 (2021).
[45]Y. L. Raikher, V. V. Rusakov, and R. Perzynski, Soft Matter **9**, 10857 (2013).
[46]L. H. Cai, S. Panyukov, and M. Rubinstein, Macromolecules **44**, 7853 (2011).
[47]Y. Kanakubo, C. Watanabe, J. Yamamoto, N. Yanagisawa, H. Sakuta, A. Nikoubashman, and M. Yanagisawa, ACS Mater. Au **3**, 442 (2023).
[48]C. C. Miller, Proc. R. Soc. London, Ser. A **106**, 724 (1924).
[49]H. Qian, M. P. Sheetz, and E. L. Elson, Biophys. J. **60**, 910 (1991).